JOURNAL OF MATERIALS SCIENCE **35** (2000) 1087–1096

Crack formation in sapphire/niobium/sapphire joints under compression

G. SOYEZ, G. ELSSNER, M. RÜHLE
Max-Planck-Institut für Metallforschung, D-70174 Stuttgart, Germany
E-mail: soyez@mf.mpi-stuttgart.mpg.de

R. RAJ
University of Colorado, Boulder, CO 80309-0427, USA

Compression tests were carried out on UHV diffusion bonded single crystalline sapphire/Nb/sapphire joints to investigate their mechanical properties, the mechanisms that lead to the failure of the joints and the dislocation-interface interaction. The tests were performed for different orientation relationships (OR) at the interface to study the influence of different bond strength on the mechanical behavior. Additionally, the metal layer thickness was varied for each OR to alter the influence of the interface. The experimental results showed, that with decreasing metal layer thickness the stress needed to form a crack increases drastically, whereas for the Nb/sapphire system the bond strength at the interface seems to have no significant influence on the mechanical behavior of the joint. A theoretical model will be presented that explains the experimentally observed relationship between metal layer thickness and crack stress.

1. Introduction

Metal/ceramic interfaces play an important role in many technological areas and industrial applications such as electronic packaging systems, thin film technology, protective coatings and structural metal/ceramic composites. However, the microscopic processes in the vicinity of metal/ceramic interface during mechanical loading have been only poorly investigated. The intent of the present work is to study for a metal/ceramic model system the interaction of the dislocations with the interface during the plastic deformation of the metal. Fig. 1 shows some ways how dislocations can interact with a metal/ceramic interface: (a) dislocations running into the interface may change their direction and move parallel to interface which is easily possible for screw dislocations in bcc metals due to cross-slip mechanisms; (b) dislocations are reflected at the interface due to different elastic constants; (c) dislocations cause a cleavage crack at the interface due to a pile-up; (d) a pile-up of dislocations yields to a crack formation in the ceramic.

For the present investigation the model system Nb/sapphire has been selected because both materials possess similar thermal expansion coefficients, so that residual stresses at the interface after the bonding procedure are minimized. Furthermore, the interface between Nb and sapphire is well characterized in terms of structure and mechanical properties. In a previously published work, the elastic and yield behavior of the joints in compression have been reported [1]. The present study will concentrate on the fracture mechanisms leading to the failure of the sapphire/Nb/sapphire joints.

2. Experimental details

Sapphire/Nb/sapphire sandwiches were prepared by diffusion bonding in a machine described elsewhere [2]. The preparation of the single crystals prior to bonding and the subsequent preparation steps to get compression samples are described in a previous work [1]. The bonding of the specimens was carried out by heating the stack of specimens to the bonding temperature of 1400°C within 1.5 h, holding this temperature for 3 h and then cooling to room temperature in another 1.5 h. After reaching the bonding temperature a pressure of about 7 MPa was applied to the stack of specimens. The diffusion bonded samples were cut into several compression test specimens by means of a diamond saw. The compression specimens had lengths between 5 and 8 mm and a square cross section with a specimen width $a \approx b$ of 3.8 ± 0.3 mm. The edges of the specimen were rounded to minimize the influence of edge effects.

The small specimen size required a special device (Fig. 2) to carry out the compression test. A detailed description of the device and the evaluation of the load-strain data can be found in [1]. The sapphire/Nb/sapphire tricrystals (TCC: tri-crystal-combination) were tested with the metal/ceramic interfaces perpendicular to the loading axis.

Table I shows the investigated ORs between Nb and sapphire and their interface strengths, characterized by the fracture energy G_c in 4-point bending [3]. Two important facts should be pointed out: (i) the single crystals in the stack were orientated so that the same OR holds at both Nb/sapphire interfaces; (ii) for TCC1

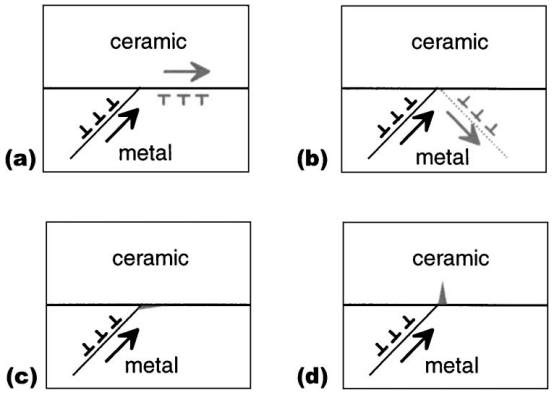

Figure 1 Possible interactions of dislocations with a metal/ceramic interface during plastic deformation of the metal: (a) dislocation change direction and run parallel to the interface; (b) dislocations are reflected; (c) formation of a cleavage crack at the metal/ceramic interface due to dislocation pile-up; (d) pile-up of dislocations at the interface initiates crack in ceramic.

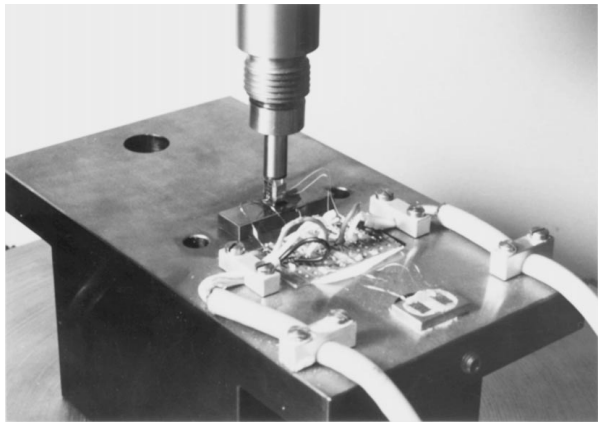

Figure 2 Micrograph of the device used for the compression tests. The sample has dimensions of approximately $8 \times 4 \times 4$ mm^3.

to TCC3 different interface strengths were realized by bonding differently orientated sapphire crystals to the $\{110\}_{Nb}$-plane. Hence the deformation mode and the activated slip systems in the Nb should be the same for these 3 ORs.

3. Experimental results

3.1. Mechanical testing

Typical stress-strain-curves for sapphire/Nb/sapphire joints of varying metal layer thickness are shown in Fig. 3. The failure of the sapphire by crack formation is accompanied by a load drop in the stress-strain-curve, indicated by an arrow. After crack formation the loading cycle was interrupted and the specimen was removed from the device.

TABLE I Crystallographic orientation of the specimens and their fracture energies $\bar{G}_c$ [3]

Specimen	Orientation relationship	Fracture energy $\bar{G}_c$ (J/m^2)
TCC1	Nb(110)[001] $\parallel$ α-Al_2O_3(0001)[11$\bar{2}$0]	1876 ± 610
TCC2	Nb(110)[001] $\parallel$ α-Al_2O_3(000$\bar{1}$)[1$\bar{1}$00]	1899 ± 213
TCC3	Nb(110)[00$\bar{1}$] $\parallel$ α-Al_2O_3(1$\bar{1}$00)[000$\bar{1}$]	114 ± 25
TCC4	Nb(111)[1$\bar{1}$2] $\parallel$ α-Al_2O_3(0001)[1$\bar{1}$00]	112 ± 51

The crack stresses for different OR as a function of the metal layer thickness h are shown in Fig. 4. For a layer thickness larger than 2 mm the crack stress is about 120 MPa whereas for layer thicknesses of 1 mm the stress has to be increased up to 300 MPa to initiate a crack in the sapphire. The experimental results show for all ORs an increasing crack stress σ_{crack} with decreasing metal layer thickness h. A strong influence of the OR on the crack stress can't be observed.

3.2. Light microscopy

In Fig. 5 a compression specimen of the OR TCC1 is shown after crack formation in the ceramic. On the $\{110\}_{Nb}$-side face shear bands are visible, whereas the bending of the $\{100\}_{Nb}$-side face can easily be observed and is due to the plastic deformation of the Nb. These shear bands on the $\{110\}_{Nb}$-side face could be observed for all investigated ORs. The crack is restricted to the ceramic and is not continued into the metal.

To examine the crack course in the sapphire, top view photographs of the compression specimens for the four OR were taken (Fig. 6). The viewing direction is through the transparent sapphire onto the Nb bonding plane. Fig. 6 shows that the crack course is dependent on the OR at the interface. Thus for better comparison the Nb- and sapphire-directions in the bonding plane are specified.

During compression tests single cracks appeared as well as multiple cracks. For TCC1 and TCC2 the frequency of multiple cracks is equal to that of single cracks, whereas for TCC3 multiple cracks and for TCC4 single cracks dominate (see Fig. 7). The cracks appear also with similar frequency in the top and the bottom ceramic. Thus an influence of the compression device on the crack formation can be excluded.

3.3. TEM studies

Conventional TEM studies were carried out to characterize the metal/ceramic interface region before and after the compression test. Cross-sectional TEM specimens of the interface were prepared following the

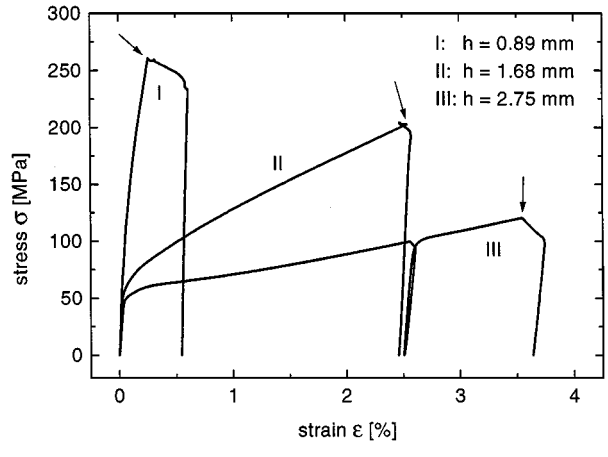

Figure 3 Stress-strain-curve for sapphire/Nb/sapphire compression specimens (OR TCC1) of different metal layer thickness. The failure of the sapphire is accompanied by a load drop indicated by an arrow.

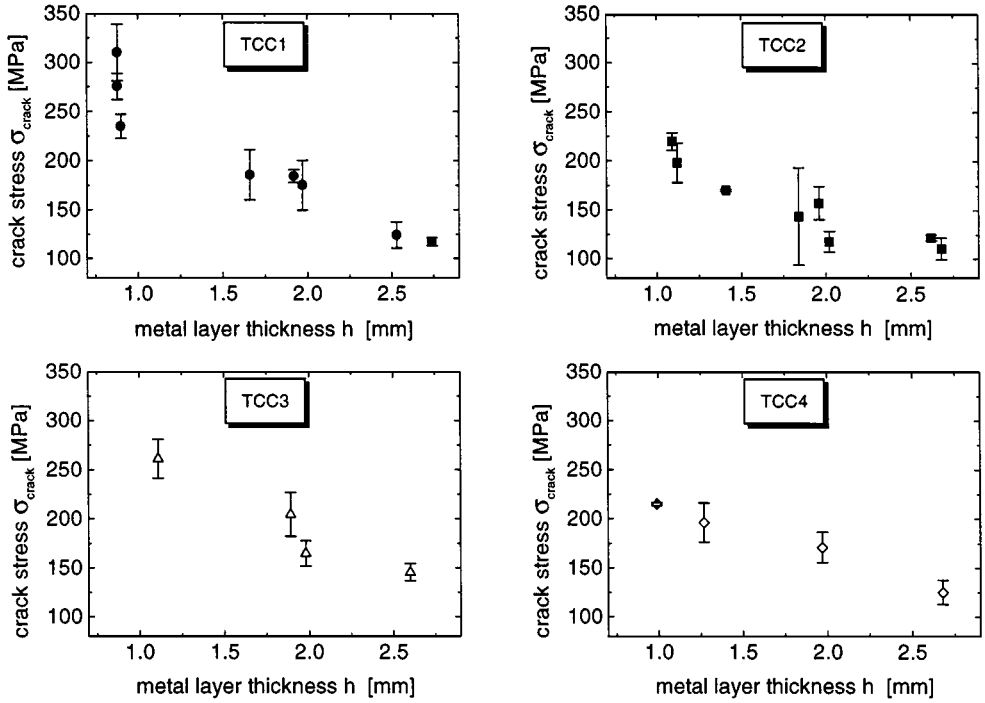

Figure 4 Crack stress of specimens TCC1 to TCC4 as a function of the metal layer thickness.

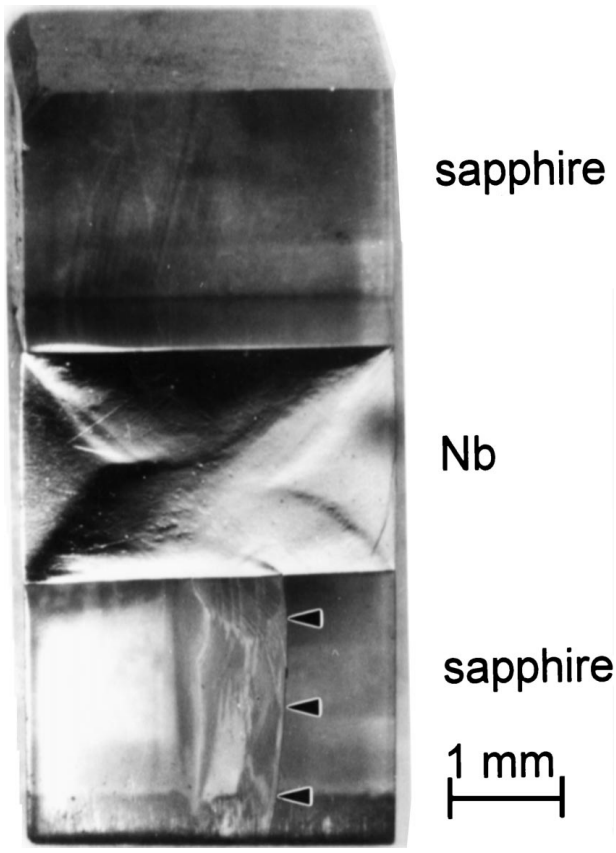

Figure 5 Compression specimen (OR: TCC1, $\varepsilon_{crack} = 2.3\%$) after crack formation in the sapphire. The crack runs perpendicular to the interface.

established procedures [4]. Fig. 8 shows a CTEM bright field micrograph of the Nb/sapphire interface region after diffusion bonding. A small-angle grain boundary can be identified close to the interface in the Nb. The small-angle grain boundaries exist within a distance of about 5 μm from the interface and have been described before [5]. They can presumably develop due to the compressive stress applied during the diffusion bonding process.

After the compression test had been carried out, TEM specimens were prepared of the interface region where the crack occurred. Due to the constraint at the interface, specimens often debonded at the interface or cracks in the sapphire developed during one of the preparation steps. However, some specimens revealed, in regions where the sapphire remained bonded to the Nb, dislocation configurations as in Fig. 9. For the interface region shown in Fig. 9, a Burgers vector analysis was performed. It revealed 4 different dislocation systems with Burgers vectors of $\{111\}_{Nb}$-type or of $\{001\}_{Nb}$-type [3], the latter probably the product of two $\{111\}_{Nb}$-dislocations reacting to form sessile $\{001\}_{Nb}$-dislocations. Dislocation arrays as in Fig. 9 appeared only in compression tested samples and hence seem to form during the plastic deformation of the metal.

4. Theoretical crack-formation model

In this section a model for the measured dependence of the crack stress σ_{crack} will be developed. Fig. 10 shows schematically the stresses acting at the metal/ceramic interface of the joint. The loading direction is parallel to the z-direction and perpendicular to the metal/ceramic interface. If only small loads are applied to the joint, the deformation is still elastic and the different Poisson's ratios of Nb and α-Al_2O_3 lead to shear stresses τ parallel to the interface [6]. These shear stresses set the ceramic under tension and the metal under compression in x-direction. At the beginning of the deformation process, the maximum shear stresses occur at the edge of the sample [7, 8]. After the plastic deformation in the metal starts, the values for τ are assumed to be constant and thus an approximately constant tension stress σ_x parallel to the interface is acting on the ceramic.

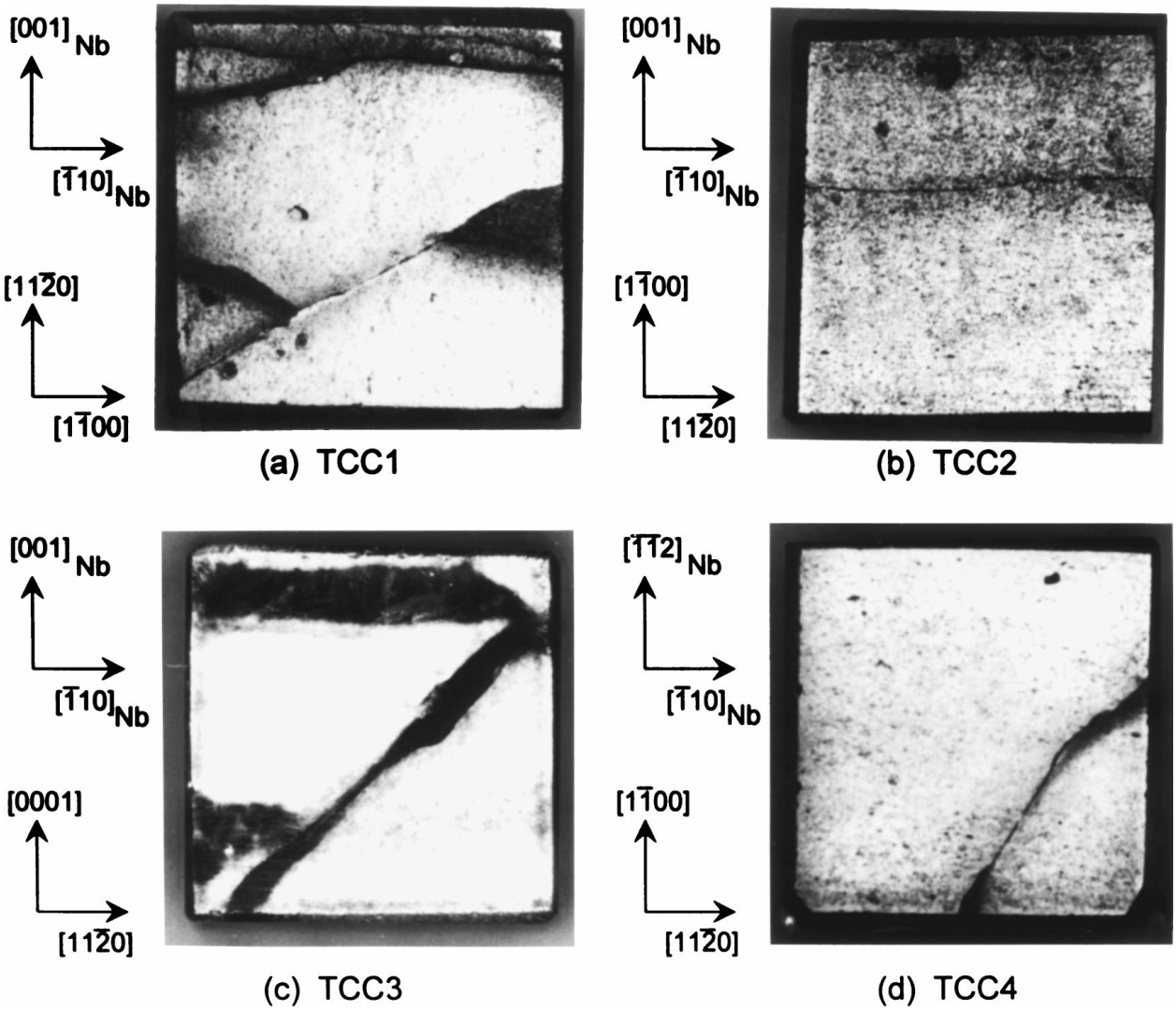

Figure 6 Top view micrograph of the crack direction in the sapphire after failure of the joints for the orientation relationships TCC1 (a); TCC2 (b); TCC3 (c); and TCC4 (d). The viewing direction is through the transparent sapphire onto the Nb bonding plane. On the left side of the micrographs the crystallographic directions in the bonding plane are given.

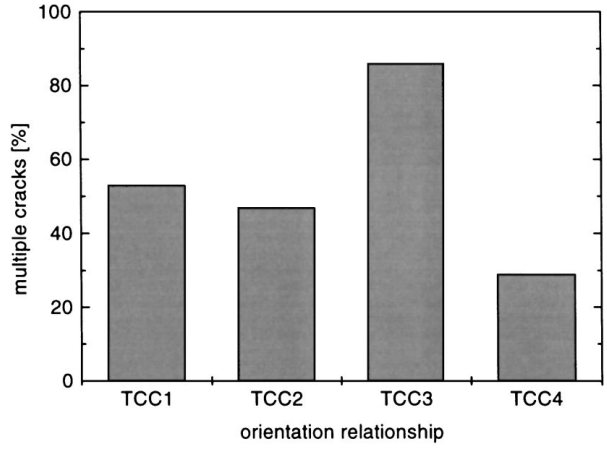

Figure 7 Percentage of multiple cracks in the sapphire after failure of the sapphire/Nb/sapphire-joints.

The occurrence of stresses perpendicular and parallel to the interface is used for the extension of a model initially developed by Cottrell [9] for the cleavage crack formation in bcc metals to that of metal/ceramic interfaces. Cottrell proposed that dislocations, operating on intersecting slip planes 45° to the tensile axis, coalesce to form a super-dislocation equivalent to a cleavage crack that is oriented perpendicular to the externally applied stress. Cottrell calculated a fracture criterion (Equation 1) which describes the equilibrium between a stable crack of finite size and a cleavage crack growing indefinitely.

$$p \cdot n\boldsymbol{b} = 2\gamma. \tag{1}$$

p denotes the applied tension stress, $n \cdot \boldsymbol{b}$ is the Burgers vector of the super-dislocation with n as the number of dislocations that coalesce to form the crack, and γ is the surface energy of the metal.

Cottrell's fracture criterion will now be extended to describe the crack behavior of metal/ceramic interfaces in compression. During the plastic deformation of the metal, dislocations are moving into the direction of the interface. Because of the lack of plasticity of the ceramic under room temperature conditions, they will be piled up at the interface (see Fig. 11).

The stress at the tip of the pile-up is proportional to the number n of piled up dislocations and the shear stress acting on the dislocations. To estimate the number of piled up dislocations that can occupy a distance L along a slip plane, the Eshelby-Frank-Nabarro [10]

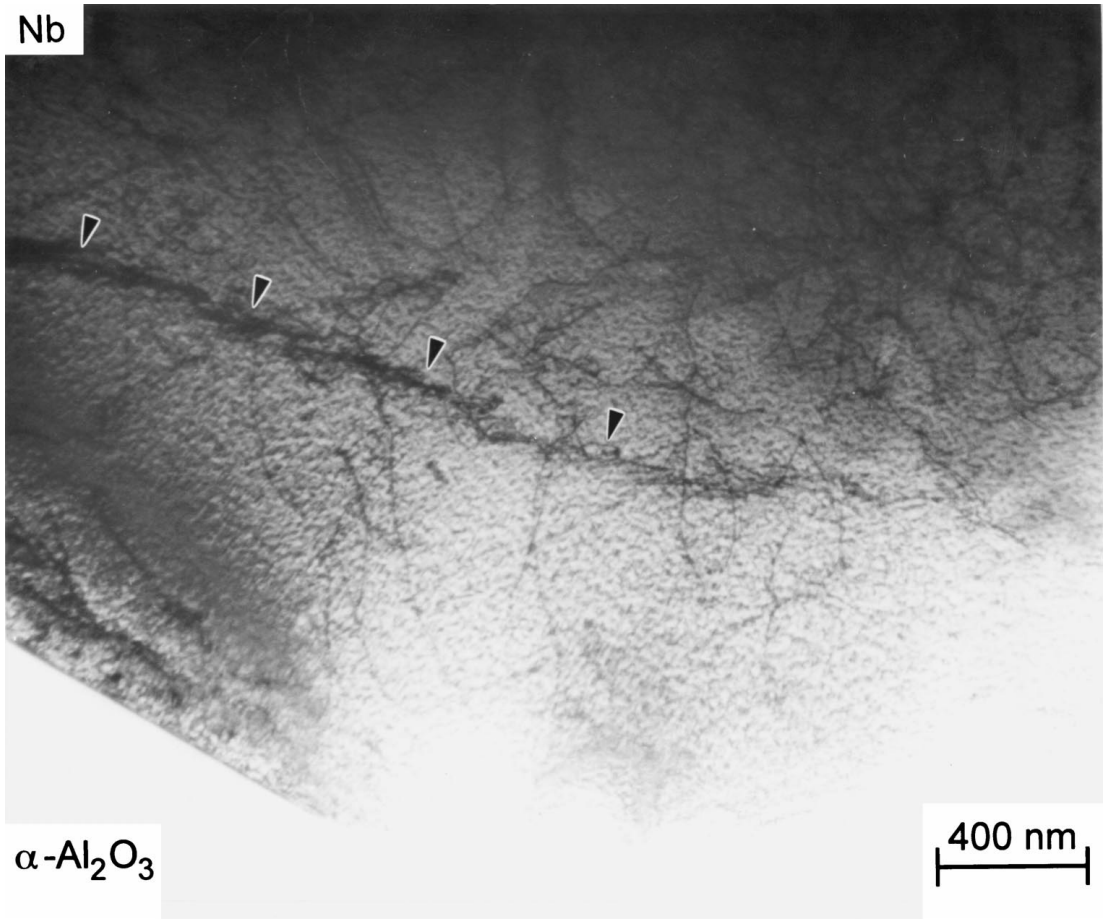

Figure 8 CTEM bright field image of the Nb/sapphire interface in the as-diffusion bonded state. In the Nb a small-angle grain boundary can be observed at a distance of about 1 μm from the interface.

expression will be used,

$$n = \frac{\pi \cdot (1-\nu) \cdot L \cdot \tau_{\text{eff}}}{G \cdot \boldsymbol{b}}. \tag{2}$$

The number n is dependent on the shear modulus G, the Poisson's ratio ν and the effective shear stress τ_{eff}. Using Equation 2, Equation 1 can be expressed in terms of the pile-up length L and the effective shear stress acting on the dislocations

$$p \cdot \frac{\pi \cdot (1-\nu) \cdot L \cdot \tau_{\text{eff}}}{G} = 2\gamma. \tag{3}$$

Equation 3 is a fracture criterion based on the surface energy of the fracturing material, the potential length of piled up dislocations, the stress acting on the dislocations and the applied tensile stress acting on the crack.

To compare this model with the experimental data, some idealizing assumptions have to be made:

- The maximum pile-up length is reached, if the dislocation source is located in the middle of the metal layer. Thus L is chosen to be half of the metal thickness.
- The effective shear stress acting on the dislocations in the slip plane is the result of the applied stress and the mechanisms hindering the dislocation movement. Such mechanisms are for example the interaction of dislocations with phonons, lattice defects, precipitates and the interaction between the dislocations themselves. Furthermore, the movement of the dislocations is hindered by the so-called Peierls barrier. The Peierls barrier has its origin in the periodicity of the crystal lattice and describes the resistance that has to be overcome before dislocation movement can take place. All these mechanisms reduce the effective stress acting on a dislocation. As an upper limit for all these different processes hindering dislocation motion the uniaxial yield stress will be used. The effective stress in the slip plane is thus estimated by half of the difference between the crack stress σ_{crack} and the uniaxial yield stress σ_0.
- The stress p acting in x-direction is equivalent to the tension stress σ_x.

These assumptions are summarized in the following expressions:

$$L = \frac{h}{2}; \quad \tau_{\text{eff}} = \frac{1}{2}(\sigma_{\text{crack}} - \sigma_0); \quad p = \sigma_x \tag{4}$$

Substituting Equation 4 into Equation 3 yields a formula which gives the variation of the crack stress σ_{crack} on the metal layer thickness:

$$\sigma_{\text{crack}} = \sigma_0 + \frac{8 \cdot G \cdot \gamma}{\pi \cdot (1-\nu) \cdot \sigma_x} \cdot \frac{1}{h} = \sigma_0 + \Omega \cdot \frac{1}{h} \tag{5}$$

Equation 5 demonstrates that the crack stress is inversely proportional to the metal layer thickness. The quantity σ_0 is consistent with the uniaxial yield stress of the metal, whereas the parameter Ω is dependent on the elastic constants G and ν of the metal, the surface

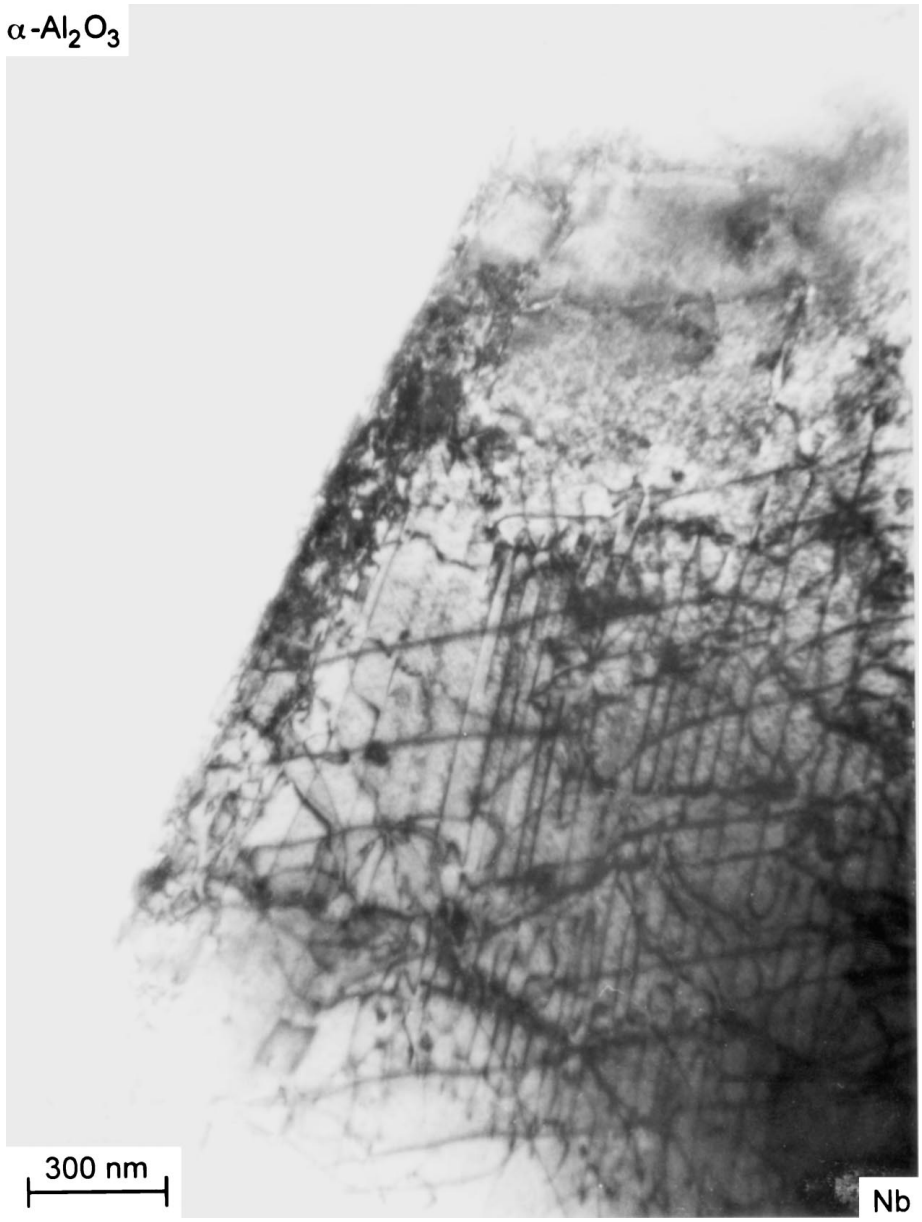

Figure 9 CTEM bright field image of a Nb/sapphire interface region after a compression test was carried out (OR: TCC1; $\varepsilon_{crack} = 2.3\%$).

energy γ of the ceramic and the tension stress σ_x acting on the ceramic parallel to the interface. The simplifying assumptions which form the basis for the proposed model suggest that Equation 5 is a lower limit for the dependence of the crack stress on the metal thickness.

5. Application of the model to experimental crack stresses

The previously described model will now be used to explain the dependence of the metal layer thickness on the measured crack stresses. Since there were no significant differences between the four OR TCC1 to TCC4 (see Table II), all data are plotted together in Fig. 12.

The linear relationship between crack stress and reciprocal metal thickness of the developed model is confirmed by the experimental data. In Fig. 12, the straight line named σ_{fit} was obtained by a linear regression over all data points (TCC1 to TCC4) and is plotted together with the upper and lower limit of the simulation.

The parameter Ω can be calculated if the terms in Equation 5 are known. The elastic constants can be

TABLE II Results for the linear regression for the different orientation combinations. Shown are the two fit parameters $\sigma_{0,fit}$ and Ω_{fit} (compare Equation 5) as well as the linear regression coefficient R

Orientation relationship	$\sigma_{0,fit}$ (MPa)	Ω_{fit} (MPa · mm)	R (%)
TCC1: Nb(110)[001] ∥ α-Al_2O_3(0001)[$11\bar{2}0$]	66 ± 22	187 ± 27	94
TCC2: Nb(110)[001] ∥ α-Al_2O_3(0001)[$1\bar{1}00$]	48 ± 14	176 ± 22	96
TCC3: Nb(110)[001] ∥ α-Al_2O_3($1\bar{1}00$)[0001]	67 ± 29	219 ± 47	96
Mean of TCC1 to TCC3	58 ± 15	190 ± 21	91
TCC4: Nb(111)[$\bar{1}\bar{1}2$] ∥ α-Al_2O_3(0001)[$1\bar{1}00$]	90 ± 22	129 ± 31	95
Mean of TCC1 to TCC4 ($\Rightarrow \sigma_{fit}$)	63 ± 13	180 ± 19	91

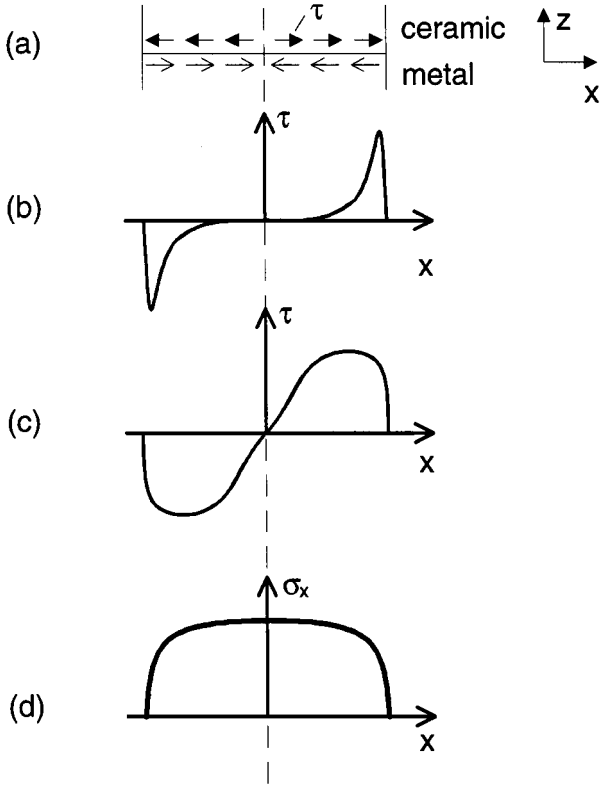

Figure 10 Schematic presentation of the (a) stresses parallel to the metal/ceramic interface for different stages of the compression test; (b) elastic compression of the bicrystal in z-direction; (c) plastic deformation of the metal and the resulting tensile stress σ_x; (d) in the ceramic parallel to the interface.

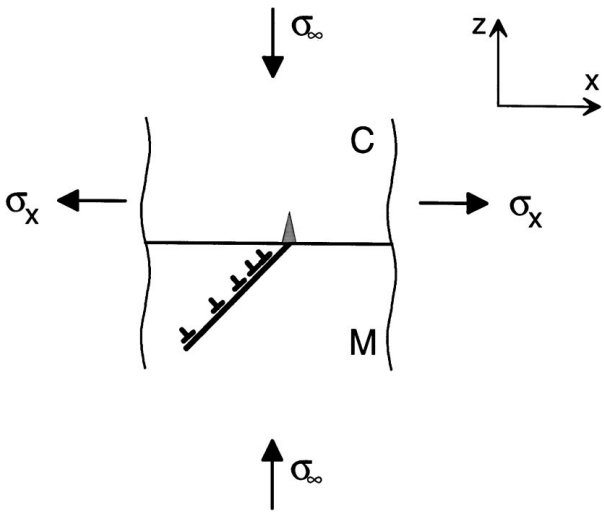

Figure 11 Model for the crack initiation after plastic deformation of the metal by a dislocation pile-up at the metal/ceramic interface. σ_∞ denotes the externally applied stress and σ_x the stress acting on the ceramic due to the plastic deformation of the metal.

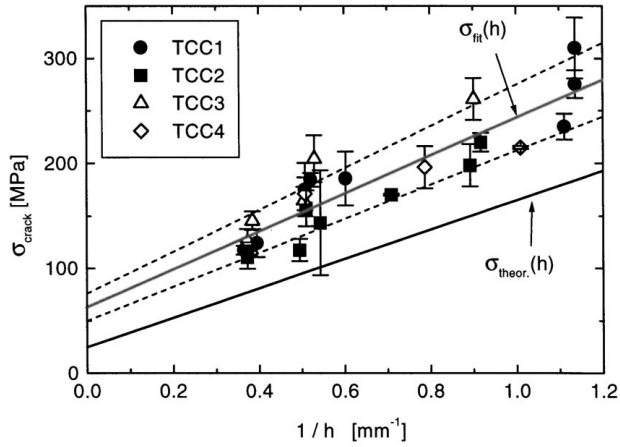

Figure 12 Crack stress σ_{crack} in dependence of the reciprocal metal layer thickness. The straight lines obtained by linear regression ($\sigma_{fit}(h)$: $\sigma_{0,fit} = 63$ MPa, $\Omega_{fit} = 180$ MPa · mm) and by using literature data to calculate Ω ($\Omega_{theor.}(h)$: $\sigma_0 = 25$ MPa, $\Omega_{theor.} = 140$ MPa · mm) are added to the plot.

obtained for the required directions by using a method described by Turley and Sines [11]. Instead of the theoretical surface energies of sapphire in the order of 1.4 J/m^2 to 2.6 J/m^2 [12] experimentally measured fracture energies γ_b for sapphire were used. These values are much higher than the theoretical calculated surface energies due to dissipative processes during cracking [13]. The fracture energies in sapphire for the suitable cleavage planes vary between 6 J/m^2 and 9 J/m^2 [14–16]. As a mean value for the fracture energy γ_b was chosen to be 7 J/m^2 (compare Table V). The stress σ_x was estimated by the absolute value of the shear stress τ. For this shear stress either the literature values of the critical resolved shear stress can be used or the values for the shear stress k parallel to the interface, which were obtained with the model describing the plastic behavior of the joints [1]. In Table III, the calculated values for $\Omega_{theor.}$ and the values received by linear regression are listed. Using the values for σ_0 and $\Omega_{theor.}$ (see Table III) leads to the straight line named $\Omega_{theor.}$ in Fig. 12.

Table III shows that by estimating Ω using the critical resolved shear stress τ_{crss} the calculated values agree quite well with the measured ones, whereas inserting the shear stresses k obtained with the model describing the yield behavior [1] leads to values for $\Omega_{theor.}$ which are too low. This implies that the crack stress is only determined by the metal layer thickness and the fracture energy of the sapphire. Table II and the estimation for Ω (see Table III) prove that different bond strengths have no influence on the crack stress in the Nb/sapphire system. The values obtained for the parameter $\sigma_{0,fit}$ are about twice the uniaxial yield stress of Nb [1].

TABLE III Calculated values for the parameter Ω using data from the literature and comparison with the experimental values

Specimen	Fracture energy γ_b (J/m^2)	G_{Nb} (GPa)	ν_{Nb}	σ_x (MPa) $\lvert\sigma_x\rvert \approx \lvert\tau\rvert$	$\Omega_{theor.}$ (MPa · mm)	Ω_{fit} (MPa · mm)
		{110}⟨111⟩		τ_{crss} k		
TCC1 to TCC3	∼7	41.8	0.47	10 27	140 . . . 52	190 ± 21
		{110}⟨uvw⟩		τ_{crss} k		
TCC4	∼7	41.8	0.42	10 22	128 . . . 58	129 ± 31

6. Discussion

6.1. Crack formation model

The results in the previous section show, that the experimentally observed crack stress σ_{crack} of the joints can be explained by the theoretical crack-formation model. The assumptions for the derivation of Equation 5 lead to a lower limit for the crack stress in dependence of the metal layer thickness. Applying the model to the measured data leads to a yield stress σ_0 which is twice as high as the yield stress of bulk Nb. However, in the model the yield stress σ_0 is used to describe all effects that can hinder the movement of the dislocations in the metal. So far, an impediment of the dislocation movement at the near interface region due to interstitially dissolved oxygen in the Nb was not considered. This oxygen uptake of the niobium during the bonding process was estimated by Korn [17] through hardness measurements and a chemical analysis of the bulk niobium before and after bonding to be 0.1 at.%. This oxygen uptake leads, by using the strengthening rates of Elssner [18] and Leadbetter [19] of 350 MPa per at.% oxygen, to an increase of the yield stress $\Delta\sigma$ of 35 MPa. The values $\sigma_{0,\text{fit}}$ calculated with the presented model are about 60 MPa and are of the order of the yield stress σ_0 plus the increase in the yield stress $\Delta\sigma$ in the near interface region due to the oxygen uptake

$$\sigma_{0,\text{fit}} \approx \sigma_0 + \Delta\sigma.$$

A further indication of an impediment of the dislocations in the vicinity of the interface are given by the observed slip traces on the Niobium, as shown in an earlier publication [1]. On the polished $\{110\}_{\text{Nb}}$-side faces slip traces were visible near the interface. These traces discharged into the bright band running parallel to interface. In the region between the Nb/sapphire interface and this bright band no slip traces were found which means that the movement of dislocations is hindered, for example through to a higher oxygen content in this region. Together with stresses caused by different Poisson's ratios these are processes increasing the necessary stress to induce dislocation movement. The observed dislocations with Burgers vectors parallel to the $[100]_{\text{Nb}}$-direction may result from the dislocation reaction of two $\langle 111\rangle_{\text{Nb}}$-dislocations and thus form the nucleation site for the microcrack that initiates the fracture of the sapphire.

The calculated values for $\Omega_{\text{theor.}}$ using literature data are in good agreement with the values obtained with the developed model. The use of fracture energies instead of the theoretical surface energies is reasonable since in the experiments the experimental fracture energies are decisive for the crack initiation in the sapphire. The main uncertainty lies in estimation of σ_x. This stress is given by the integration over the shear stress τ acting along the interface. Strictly speaking, σ_x is not constant and has a maximum in the middle of the sample. The exact functional relationship between σ_x and τ is not known. The estimation of τ by means of the critical resolved shear stress in Niobium is only a rough approximation. Furthermore, it is necessary to take into account that during the crack formation in the sapphire the stress normal to the crack direction is decisive. For this reason, cracks with cleavage planes not perpendicular to the metal/ceramic interface experience a reduced effective stress acting on them.

As observed for the yield behavior of the joints [1], an influence of the bond strength at the metal/ceramic interface on the crack behavior could not be detected. For the investigated Nb/sapphire joints the bond strength at the interface, characterized by the fracture energy $\bar{G}_c$, is even for the weaker OR in the order of 100 J/m^2, and thus very high. This might be the reason why increasing the bond strength further does not have any measurable effect on the crack stress.

6.2. Crack path in the ceramic

The crack formation in the ceramic during the compression test raises the question as to how the crack is initiated. One possibility is, that according to the model described in this study the crack formation is caused by a dislocation pile-up. Another possibility is the nucleation of the crack through the stress σ_x parallel to the interface acting on microcracks and flaws in the ceramic. The answer to this question is hard to obtain by CTEM, since the compression test can't be stopped at the moment of crack formation but will be continued for some tenths of a second. Because the edges of the cracks are pushed into the metal, new dislocations will form. An investigation of the dislocation arrangement in the crack region after crack formation by CTEM thus makes it impossible to decide whether the dislocations initiated the crack or whether they were formed after the crack in the sapphire appeared.

More illuminating is the investigation of the traces of the forming cleavage planes of the sapphire and comparing them with the primary slip systems in niobium. In Fig. 13 the traces of the crack planes of sapphire and the traces of the primary slip systems in Nb in the interface are shown. Fig. 13 shows schematically the experimentally observed cracks of Fig. 6. At an angular range of $\pm 5^\circ$ there is an existing primary slip system in the Nb that can explain the observed crack in the sapphire by a pile-up of dislocations. These results are summarized in Table IV. The fracture energies for

TABLE IV Comparison between experimentally observed crack directions and the traces of the cleavage planes of sapphire

Specimen	Observed angle with $[\bar{1}10]_{\text{Nb}}$	Frequency (%)	Cleavage planes in sapphire	Angle with $[\bar{1}10]_{\text{Nb}}$
TCC1	$\pm 5^\circ$	43	$\{11\bar{2}0\}$, $\{1\bar{2}13\}$	0°
	24°–34°	30	$\{1\bar{1}00\}$, $\{10\bar{1}2\}$	30°
TCC2	$\pm 5^\circ$	83	$\{1\bar{1}00\}$, $\{10\bar{1}2\}$	0°
TCC3	$\pm 5^\circ$	38	$\{10\bar{1}2\}$	0°
	40°–45°	38	$\{1\bar{2}13\}$	42.3°
TCC4	60°	80	$\{1\bar{1}00\}$, $\{10\bar{1}2\}$	60°, 0°
	30°		$\{11\bar{2}0\}$, $\{1\bar{2}13\}$	30°

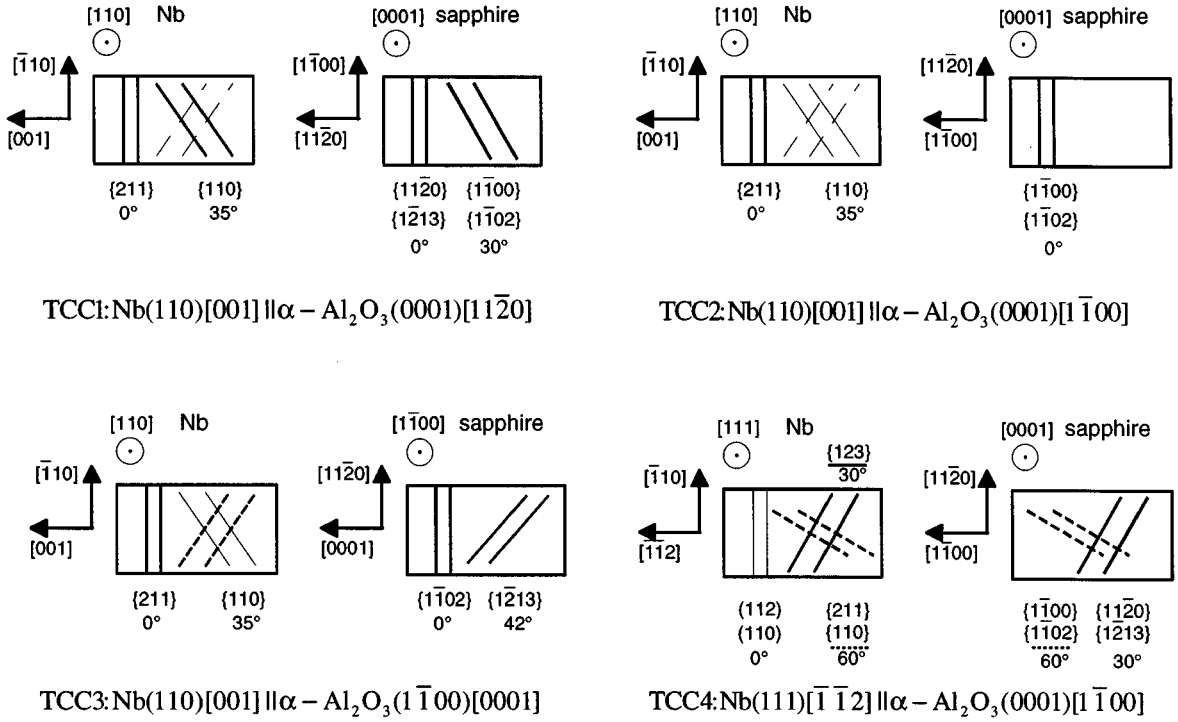

Figure 13 Traces of the observed cracks in the sapphire and the primary slip systems in Nb in the bonding plane for the OR TCC1 to TCC4. The angles given are in respect to the $[\bar{1}10]_{Nb}$-direction. The bold lines in the Nb plane mark the slip systems that are most likely to cause the observed cracks in the sapphire.

TABLE V Experimentally observed fracture energies for different cleavage planes in sapphire by Wiederhorn [14] and Becher [16]

	Energy γ_b (J/m^2)	
Cleavage plane	Wiederhorn [14]	Becher [16]
{1$\bar{1}$00}	7.3	8.8
{11$\bar{2}$0}		6.7
{10$\bar{1}$2}	6.0	
{1$\bar{2}$13}		6.8
(0001)	>40	>30

different cleavage planes measured by Wiederhorn [14] and Becher [16] are listed in Table V. Because of their similarity all cleavage planes should show up with equal frequencies. The only exception is the densest packed basal plane with a very high cleavage energy, but the cleavage on {0001}-planes could not be observed, compare Table V.

Crack formation due to dislocation pile-up in the Nb at the interface is also confirmed by a more detailed analysis of the observed crack paths for OR TCC1 and TCC2. For these ORs the potential cleavage planes have a 60°-rotational symmetry, but no cracks perpendicular or with an angle of 60° to the $[110]_{Nb}$-direction were observed.

To ensure that the crack formation during the compression test is not initiated at the anvil/sapphire interface, test were performed on bulk sapphire samples which were polished and prepared the same way as the ones used for diffusion bonding. The samples were loaded up to maximum applicable stress of the load cell which was about 600 MPa. Although these tests were carried out with and without lubrication between sample and anvil, no cracks could be initiated in the sapphire. This leads to the conclusion that the cracks

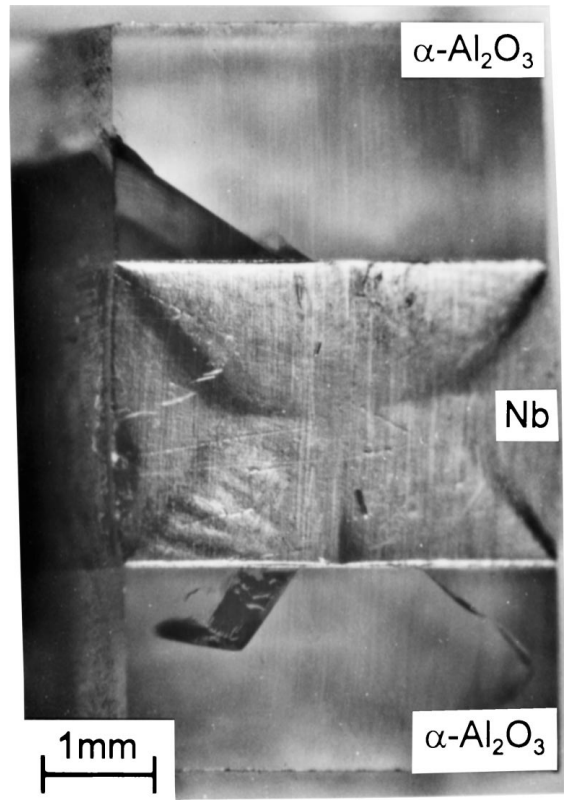

Figure 14 Micrograph of a compression specimen of OR TCC3 after crack formation ($\varepsilon_{crack} = 1.8\%$). The cracks are initiated at the interface and run to the side faces due to the activated cleavage planes.

are initiated by local stress concentrations caused by a pile-up of dislocations at the interface, which is also supported by the observed crack path for OR TCC3. For this OR, the sapphire has no potential cleavage planes perpendicular to the interface Fig. 14 shows that the cracks start at the interface.

7. Conclusions

The present studies of the mechanical behavior of single crystalline sapphire/Nb/sapphire joints were carried out to examine the interaction between dislocations and the interface during plastic deformation of the metal. The experimentally observed crack stress of the ceramic is inversely proportional to the metal layer thickness, whereas the bond strength at the interface has no significant influence on the mechanical properties for the Nb/sapphire model system. The extension of Cottrell's model for the crack formation in bcc metals to metal/ceramic interfaces describes the observed crack formation and the accompanying crack stress reasonably well. The present results indicate, that the crack formation in the sapphire is caused by a dislocation pile-up at the metal/ceramic interface. This assumption is supported by the correlation between the slip systems in the Nb and the traces of the occurring cracks in the sapphire.

Acknowledgment

The authors would like to thank Prof. D. Conway at Cornell University (Cornell) for helpful discussions.

References

1. G. SOYEZ, G. ELSSNER, M. RÜHLE and R. RAJ, *Acta Mater.* **10** (1998) 3571.
2. H. F. FISCHMEISTER, G. ELSSNER, B. GIBBESCH, K.-H. KADOW, F. KAWA, D. KORN, W. MADER and M. TURWITT, *Rev. Sci. Instrum.* **64** (1993) 234.
3. G. SOYEZ, PhD thesis, Stuttgart, 1996.
4. A. STRECKER, U. SALZBERGER and J. MAYER, *Prakt. Metallogr.* **30** (1993) 481.
5. K. BURGER, W. MADER and M. RÜHLE, *Ultramicroscopy* **22** (1987) 1.
6. A. G. EVANS, M. C. LU, S. SCHMAUDER and M. RÜHLE, *Acta Metall.* **34** (1986) 1643.
7. D. BOGY, *J. Appl. Mech.* **42** (1973) 93.
8. I. A. BLECH and A. A. LEVI, *ibid.* **48** (1981) 442.
9. A. H. COTTRELL, *Am. Inst. Min. Engrs. Trans.* **212** (1958) 192.
10. J. D. ESHELBY, F. C. FRANK and F. R. N. NABARRO, *Phil. Mag.* **42** (1959) 295.
11. J. TURLEY and G. SINES, *J. Phys. D: Appl. Phys.* **4** (1971) 264.
12. I. MANASSIDIS, A. DE VITA and M. J. GILLAN, *Surf. Sci. Lett.* **285** (1993) L517.
13. E. DÖRRE and H. HÜBNER, "Alumina" (Springer-Verlag, 1984) p. 81.
14. S. M. WIEDERHORN, *J. Am. Ceram. Soc.* **52** (1969) 485.
15. S. M. WIEDERHORN, B. J. HOCKEY and D. E. ROBERTS, *Phil. Mag.* **28** (1973) 783.
16. P. F. BECHER, *J. Am. Ceram. Soc.* **59** (1976) 59.
17. D. KORN, VDI Fortschrittsberichte Reihe 5, Nr. 320, VDI-Verlag, 1993.
18. G. ELSSNER and G. HÖRZ, *Z. Metallkde.* **62** (1971) 217.
19. M. J. LEADBETTER and B. B. ARGENT, *J. Less Comm. Met.* **3** (1961) 19.

Received 15 June
and accepted 19 August 1999